elsevier_GCA_9495

Nanoscale surface modification of Mt. Etna volcanic ashes

G. Barone[a]

P. Mazzoleni[a, *]

pmazzol@unict.it

R.R.A. Corsaro[b]

P. Costagliola[c]

F. Di Benedetto[c]

E. Ciliberto[d]

D. Gimeno[e]

C. Bongiorno[f]

C. Spinella[f]

[a]Dipartimento di Scienze Biologiche Geologiche e Ambientali – University of Catania, Corso Italia 57, 95129 Catania, Italy

[b]Istituto Nazionale di Geofisica e Vulcanologia, Sezione di Catania, Piazza Roma 2, 95123 Catania, Italy

[c]Dipartimento di Scienze della Terra – University of Florence, Via La Pira 4, 50121 Florence, Italy

[d]Dipartimento di Scienze Chimiche – University of Catania, Viale Andrea Doria 6, 95100 Catania, Italy

[e]Departament de Geoquímica, Petrologia i Prospecció Geològica – University of Barcellona, Martí i Franquès, 08028 Barcelona, Spain

[f]CNR–IMETEM, Stradale Primosole 50, 95121 Catania, Italy

*Corresponding author. Tel.: +39 0957195744; fax: +39 00957195760.

Associate editor: Lawrence M. Anovitz

Abstract

Ashes emitted during volcanic explosive activity present peculiar surface chemical and mineralogical features related in literature to the interaction in the plume of solid particles with gases and aerosols. The compositional differences of magmas and gases, the magnitude, intensity and duration of the emission and the physical condition during the eruption, strongly influence the results of the modification processes. Here we report the characterization of the products emitted during the 2013 paroxysmal activity of Mt. Etna. The surface features of the ash particles were investigated through X-ray photoelectron spectroscopy (XPS) and Transmission electron microscopy (TEM) allowing the analysis at nanometer scale. TEM images showed on the surface the presence of composite structures formed by Ca, Mg and Na sulphates and halides and of droplets and crystals of chlorides; nanometric magnesioferrite and metallic iron dendrites are observable directly below the surface. From the chemical point of view, the most external layer of the volcanic glassy particles (<5 nm), analysed by XPS, presents depletion in Si, Mg, Ca, Na and K and strong enrichment in volatile elements especially F and S, with respect to the inner zone, which represents the unaltered counterpart. Below this external layer, a transition glassy shell (thick 50–100 nm) is characterized by Fe, Mg and Ca enrichments with respect to the inner zone. We propose that the ash particle surface composition is the result of a sequence of events which start at shallow depth, above the exsolution surface, where gas bubbles nucleate and the interfaces between bubbles and melt represent proto-surfaces of future ash particles. Enrichment of Ca, Mg and Fe and halides may be due to the early partition of F and Cl in the gas phase and their interaction with the melt layer located close to the bubbles. Furthermore the formation of volatile SiF_4 and KF explain the observed depletion of Si and K. The F enrichment in the external ~50 nm thick layer of the glassy particles suggests the resorption of this element during the rise from depth less than 400 m below the summit vent. During the eruption, the gas/ash interaction persists inside the plume where further changes on the particle surface

occurs. Gaseous S, Cl and F react causing the formation of solid Ca, Mg, Na and K compounds, while SiF_4 was released as volatile phase and HF was physisorbed. Finally, in the low temperature plume zone, halides previously formed continuously react with gases producing sulfates.

1 Introduction

Chemical and mineralogical compositions of tephra are strongly influenced by their interaction with gases and/or aerosol (Rose, 1977). In particular, dry and wet deposition–adsorption of sulphur, chlorine, fluorine and metals are imputed to have a key role in changing the solid particle surface (Delmelle et al., 2007). However, the processes occurring on ashes surface during an eruption are very complex and, according to Witham et al. (2005), are controlled by numerous factors (i.e. magma composition, eruptive style, particle-gas ratio, particle grain-size and surface area, physical and chemical condition during the permanence of solid particles in the plume, environmental conditions and so on). Óskarsson (1980) proposed a simplified plume model in which ash reacts in different way as function of the gas plume temperature. In particular he recognized three different zones in the plume: (i) the salt formation zone in which gases form salt particles at nearly magmatic temperature; (ii) the surface adsorption zone where halogen gases react directly with the surface of ash at ~700 °C; (iii) the condensation zone, in which sulphuric and halogen acids, are adsorbed onto ash particles at temperatures below 338 °C. However, in this scenario, the contribution of the aforementioned factors in modifying the ash surface is not yet clear (Mather et al., 2003) even if the variability of the products emitted by different volcanoes (Ayris and Delmelle, 2012a) or by the same volcano in different eruptive conditions (Gislason et al., 2011) is well documented.

The approach normally used to study the chemical modification of solid particles surface has been based on indirect investigation such as the analysis of the release of chemical components during leaching experiments with distilled water or other solvents (Toutain et al., 1995; Ruggieri et al., 2010; Ayris et al., 2013). Recently the direct measurements and/or observation of the ash surface have been performed by XPS, atomic force microscopy and TEM analysis, furnishing new insights into the definition of the surface processes of solid particles (Delmelle et al., 2007; Gislason et al., 2011; Ayris et al., 2013, 2014; Olsson et al., 2013). These techniques overcome the limitations of the more traditional microscopic and diffractometric measurements as these do not permit investigation of nanoscale features.

In recent years, the chemical modifications experienced by ash particles surface have attracted a growing scientific interest in light of the possible impact on human health especially for high magnitude explosive volcanic activity that injects large quantities of fine grained ash in the atmosphere on global scale. However, more frequent episodes with lower magnitude may have stronger impacts in more localised areas (Africano and Bernard, 2000; Ayris and Delmelle, 2012a) that may be densely populated as in the case of the Mt. Etna slopes. In this case, the impact of tephra on the ground, can affect aspects such as buildings, lifelines and economy or the environment (Biass et al., 2014); for example, the presence of Mt. Etna ash in the atmosphere has been able to damage air traffic with the temporary closure of the Catania international airport. Finally, even if the low abundance of <10 μm grain size fraction suggests a negligible interaction between ash and the respiratory system, accurate epidemiologic studies and mineralogical and geochemical investigations are necessary to exclude detriments for the health (Fano et al., 2010).

Mt. Etna is one of the most active volcanoes in the world and in recent times it has been characterized by frequent summit eruptive activity. In particular, starting from 2011, the New South East Crater (hereafter NSEC), one of the four summit craters of the volcano, produced 'episodic' eruption, consisting of recurrent lava fountains, generally associated with lava flow emissions, lasting from a few weeks to months (Andronico and Corsaro, 2011). Episodic eruptions at NSEC occurred in 2011–12 (25 episodes from January 2011 to April 2012; Behncke et al., 2014) and most recently (19 episodes from February up to early December 2013; Bonaccorso et al., 2014).

Although these paroxysmal events have shown different characteristics in terms of magnitude, duration and eruptive styles (Andronico et al., 2014), as a common feature, they all produced an eruption plume associated with a tephra fallout event which was recorded at different distances from the NSEC eruptive center.

The occurrence of several lava fountains at NSEC in the period February to April 2013 allowed a sampling campaign of the fallout deposits formed during different paroxysms, at different distance from the NSEC. These circumstances allowed us to analyze the surface chemical and mineralogical changes of solid particles forming the tephra with different techniques, and to interpret the results in terms of the possible interaction of solid particles with gases and aerosols formed during paroxysmal events, both in the conduits and in the volcanic plume.

2 Materials and methods

2.1 Sampling

The products of seven eruptive events occurring between February and April 2013, have been sampled (Fig. 1 and Table 1). The directions of the main axis of tephra dispersal of the studied deposits are prevalently E–W or ESE-WNW, with the exception of April 18 event which had N–S direction. Fallout of ashes in the sampling sites began between 2 and 4 h after the start of the eruption. The samples were collected, according to the recommendations of Stewart et al. (2013), at the same time or shortly after deposition. Special care was taken to prevent the contamination of the volcanic material with other natural (e.g., dust or ash from previous eruptions) or anthropic particulates. Furthermore, the samples have not been in contact with water either during deposition or after the sampling.

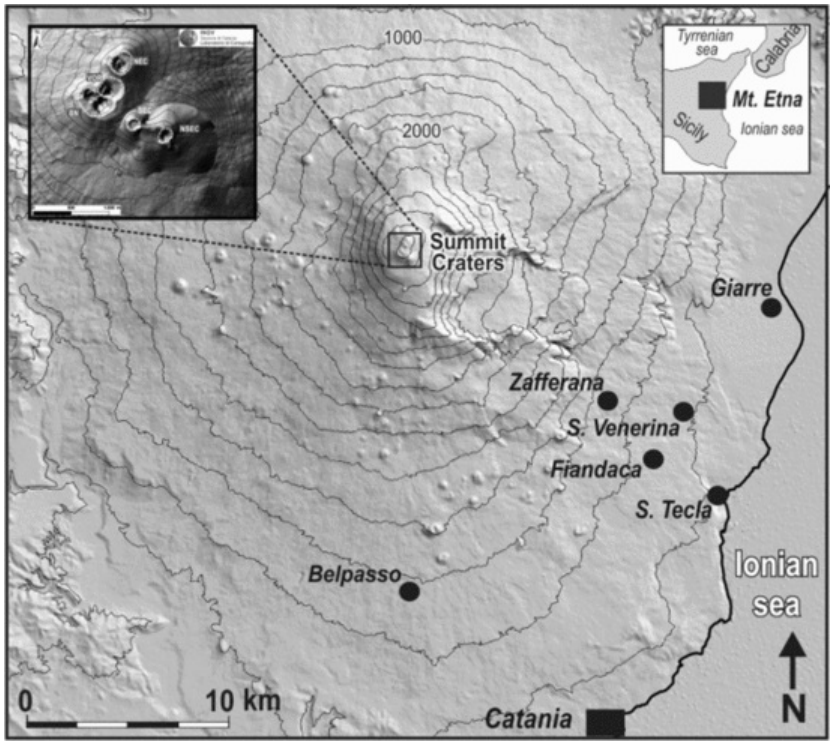

Fig. 1 Shaded relief of Mount Etna volcano with sampling sites. The inset shows the summit craters details: NEC = Northeast Crater; VOR = Voragine; BN = Bocca Nuova; NSEC = New Southeast Crater, built on the east flank of the old Southeast Crater (SEC).

Table 1 Samples of the fallout pyroclastic deposits emplaced during different eruptive episodes of NSEC in 2013. Date of eruption, locality of sampling, distance from the emission crater (NSEC) and mass per unit area are also reported.

Sample	Eruption episode	Locality of sampling	Distance from the NSEC (km)	Weight per area of the deposit (kg/m^2)
G19	02/19/2013	Giarre	17	0.9
SVEN	03/16/2013	Santa Venerina	14	8.0
STEC	04/03/2013	Santa Tecla	20	0.5
FIA	04/12/2013	Fiandaca (Acireale)	16	0.2
BEL3	04/18/2013	Belpasso	18	0.6
ZAF	04/20/2013	Zafferana	11	0.3

2.2 Grain size analysis

The size distribution of volcanic particles in the studied samples has been measured at INGV Catania, with CAMSIZER®, a laboratory instrument developed for the measurement of particle size distribution and of incoherent materials in the range 30 μm–30 mm. The sample is placed with in a vibrating feed channel and then falls through a measurement field, where images of the particles are recorded by two digital cameras with different resolutions. Images are then processed with a devoted software to provide grain-size parameters of volcanic particles (Lo Castro and Andronico, 2008).

2.3 X-ray diffraction (XRD)

X-ray powder diffraction data were provided with a Siemens D5000 diffractometer, with Cu Kα radiation and Ni filter at the Department of Biological Geological and Environmental Science of the University of Catania. An amount of 10 wt.% reference corundum standard material (NIST SRM 676a) was added to the powder to calculate the fraction of the amorphous phase. The resulting mixture was then homogenized by hand-grinding in agate mortar. Spectra were taken in the 2θ-range 3°–70°, using a step-size of 0.02°, a counting time of 5 s per step, divergence and antiscatter slits of 1° and receiving slit of 0.2 mm. Quantitative refinements have been performed according to the well-established quantitative Rietveld analysis by using GSAS program package (Larson and Von Dreele, 2000) with the EXPGUI graphical interface (Toby, 2001).

2.4 X-ray fluorescence (XRF)

Philips PW 2404/00 spectrometer was used to determine concentrations of major elements in pulverized ash samples at the Department of Biological Geological and Environmental Science of the University of Catania. Loss on ignition (L.O.I.) was gravimetrically estimated after overnight heating at 950° C. Quantitative analysis was carried out with a calibration line based on 45 international rock standards. The lower detection limits (LDL) were: SiO_2 = 1 wt.%, TiO_2 = 0.01 wt.%, Al_2O_3 = 0.1 wt.%, Fe_2O_3 = 0.05 wt.%, MnO = 0.01 wt.%, MgO = 0.02 wt.%, CaO = 0.05 wt.%, Na_2O = 0.01 wt.%, K_2O = 0.05 wt.%, P_2O_5 = 0.01 wt.%. Precision was monitored routinely by running a well-investigated in-house standard (obsidian). For all the elements, the average relative standard deviation (RDS%) is less than 5%. Accuracy, evaluated by an international standard, is <3%.

2.5 X-ray photoelectron spectroscopy (XPS)

The surface characterization of ash particles was obtained by X-ray photoelectron spectroscopy at Department of Chemical Science of the University of Catania. The analyses were performed on raw specimens and on aliquots treated by laboratory leaching. Measurements were carried out using a PE-PHI ESCA/SAM 5600 monochromator system spectrometer with an analysis chamber base pressure of 5×10^{-10} Torr.

X-ray photoemission measurements were performed using a monochromatic Al Kα (hν = 1486.6 eV) source that supplied a beam with a size of ~~7×2~~ 7 × 2 mm on the sample. The angle between the X-ray source and the hemispherical analyser was equal to 90°. Analyses were carried out with a photoelectron take-off angle of 45° and an acceptance angle of 7°. This geometry allows the investigation of more than 10 ash grains at the same time in order to have an average value of the peak intensities by reducing shape heterogeneity. On each sample, three measurements were performed on hand picked glassy ash particles identified by binocular microscope. The measured error between different analyses on the same sample did not exceed 10%. The energy scale of the spectrometer was calibrated with reference to the Ag $3d_{3/2}$ = 368.3 eV photoelectron line. Binding energies were calculated with respect to the C1s ionization at 285.00 eV from adventitious carbon that is generally accepted as independent of the chemical state of the sample under investigation (Briggs and Beamson, 1992). Quantitative analyses were performed by applying appropriate atomic sensitivity factors to the high resolution expanded bands after a subtraction of the background with the Shirley method (Fairley, 2003). The selected regions for the quantitative analyses were: C1s, O1s, F1s, Na1s, Ca2p, Al2p, Cl2p, S2p, Si2p, Mg1s, Ti 2p, K2p.

Leaching experiments were carried out according previously recommended protocols (Witham et al., 2005; Stewart et al., 2013), using Millipore ultrapure water and an ash/water ratio of 1 g: 25 ml. Each ash sample has been agitated for different duration (30, 90 and 180 min) using a shaker. During the leaching experiments, the pH variation of suspension has been measured initially every 10 s and subsequently every 60 s at room temperature of 25 °C. The initial pH of the ultrapure water (6.6) drops immediately after 10 s to 4.9 but after 30 min it rises up to 5.79 following a logarithmic trend. Successively the pH slightly increases up to 5.9 at the end of the experiment.

2.6 Transmission electron microscopy

Structural characterization of ash particles was performed by the JEOL JEM 2010 transmission electron microscope at the Catania Institute for Microelectronics and Microsystems of CNR. It is equipped with a LaB_6 thermoionic source operating at an acceleration voltage of 200 kV, a Gatan multiscan digital camera and an Oxford energy dispersive X-ray spectroscopy apparatus. The instrument achieves a spatial resolution of 0.24 nm.

The particles were inserted in a 3 mm wide copper tube, filled with two component high temperature epoxy glue. EDXS analysis of the glue identified only C, O and Na. The tube was sliced and mechanically thinned to a thickness of ~50 μm microns, and was further milled to electron transparency with an Ar ion milling system.

3 Results

3.1 Bulk characterization of ash particles

Almost all the analyzed samples show unimodal grain size curves are comprised of well-sorted coarse ash (Rose and Durant, 2009) with mode ranging between 0.5 ϕ and -0.5 ϕ, corresponding to the size class 1–1.5 mm (Fig. 2). The presence of fine ash with >0 ϕ (>1 mm) (Rose and Durant, 2009) is less than 20% in the sampled materials. The only exception is the SVEN sample which shows a negative skewed shape indicating that a high proportion of the sample is within the fine-grained tail. This sample is made of larger particles (fine lapilli), with a mode peaked at -3ϕ, corresponding to the size class 8 mm.

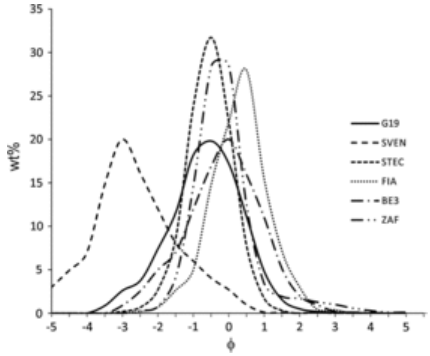

Fig. 2 Grain size distribution of the studied samples expressed as Krumbein ϕ Scale ($\phi = -\log_2 D$).

The componentry and morphology of volcanic ash particles has been observed with a stereomicroscope. All the studied samples show quite homogeneous features. About 95% of the components is made up of juvenile materials, namely sideromelane and tachilite. In particular, sideromelane particles, which are the most abundant, are vesicular, glassy, brownish coloured, with smooth surfaces. Tachylite particles are microcrystalline, blocky, with opaque and angular surfaces. The non juvenile component is rare and mostly consists of lithic clasts sub-angular in shape, frequently with altered red surfaces.

The X-ray diffractograms of the studied ash are characterized by high background and concave shape in the 10–40 2θ range, suggesting the presence of abundant amorphous volcanic glass. The abundances of crystalline and amorphous phases were dosed (Gualtieri, 2000): variable volcanic glass contents (from 99.84 wt% to 55.51 wt%) always represent the most abundant phase in all the samples (Table 2). Among minerals, plagioclase is predominant and is followed by clinopyroxene, while olivine and magnetite are only occasionally identified. No sulphates or halides were found in any analysed samples.

Table 2 Mineralogical (wt%) and chemical (major elements wt%) composition of the studied samples. For Rietveld quantitative XRD analysis are reported goodness-of-fit parameters χ^2 and R_{wp} (Toby, 2006); volcanic glass composition (wt%) measured with SEM-EDS is the average (±σ) of 10 samples from Corsaro and Miraglia (2007); n.d. = not detected, n.m. = not measured.

	G19	SVEN	STEC	FIA	BEL3	ZAF	Volcanic glass composition
X ray diffraction							
Plagioclase	10.11	21.17	28.64	0.13	6.88	33.80	
Clinopyroxene	4.32	4.03	10.91	0.03	2.48	6.92	
Glass	85.57	74.80	60.45	99.84	90.64	55.51	
Olivine	n.d.	n.d.	n.d.	n.d.	n.d.	3.63	
Magnetite	n.d.	n.d.	n.d.	n.d.	n.d.	0.14	
χ^2	1.332	1.579	1.215	1.520	1.528	1.748	
R_{wp}	0.0411	0.0542	0.0331	0.0467	0.0486	0.0503	
X ray fluorescence							
SiO_2	49.16	49.27	49.38	49.09	48.18	49.20	50.27 ± 0.79
TiO_2	2.03	2.13	2.11	2.04	1.72	1.98	2.28 ± 0.04
Al_2O_3	16.20	16.00	15.86	16.28	18.39	15.41	15.67 ± 0.25
Fe_2O_3 tot	11.96	12.08	12.45	11.87	10.08	11.92	10.59 ± 0.13
MnO	0.20	0.20	0.21	0.22	0.18	0.21	0.23 ± 0.02

MgO	3.81	3.83	3.80	3.92	4.89	3.61	2.93 ± 0.24
CaO	10.50	10.38	10.36	10.84	9.84	10.87	7.49 ± 0.37
Na_2O	3.27	3.43	3.31	3.26	3.78	3.83	4.22 ± 0.19
K_2O	1.93	1.97	2.05	1.78	1.93	2.08	4.01 ± 0.28
P_2O_5	0.35	0.28	0.38	0.31	0.48	0.30	n.m.
LOI	0.59	0.44	0.10	0.39	0.53	0.60	n.m.

The whole rock compositions of major elements in ash samples carried out by XRF (Table 2) show that all the analyzed samples are K-trachybasalts, according to the total-alkali-silica (TAS) classification diagram (Le Maitre, 2002). In particular the composition of the studied 2013 ash samples overlaps the compositional field of 2007 (Corsaro and Miraglia, 2014) and 2011–2012 (Behncke et al., 2014) products erupted during the paroxysmal activity at the South-East summit crater. Furthermore, the studied 2013 ash samples are close to the average composition of volcanic glass (Table 2) measured with SEM-EDS in quenched lavas of the 2004–05 eruption (Corsaro and Miraglia, 2007), in close agreement with the prevalence of volcanic glass in the studied samples.

3.2 Surface features

3.2.1 XPS data

The chemical composition of the external layer of ash particles was measured by XPS (Barone et al., 2014) and labeled as STEC/#, BEL3/#, G19/# and FIA/# where STEC, BEL3, G19 and FIA are the names of the selected specimens and # distinguish analyses obtained on the same sample as specified in Table 3, in which the average values of three measurements performed on different regions of each samples are reported. For comparison, the average glass composition of 2004–05 activity (Corsaro and Miraglia, 2007) is also reported. In particular, the analysis of the G19 and STEC were repeated on aliquots of the same sample with different granulometries in order to estimate any grain-size dependence on surface chemical composition. Finally, to investigate the soluble components of the ash surface, XPS analysis was performed on STEC BEL3 and FIA after leaching experiments of 30 (STEC/D; BEL3/B), 90 (BEL3/C; FIA/B) and 180 (STEC/E) minutes leaching with MilliQ ultrapure water. In Fig. 3, the exemplar XPS spectrum of the surface of STEC/B is reported.

Table 3 XPS data expressed as % Atoms; n.d. = not detected; n.m. = not measured. Bulk glass (% Atoms) composition, carried out by SEM-EDS, is from Corsaro and Miraglia (2007). Grain size is referred to the size of the analyzed particles (UL = unleached sample; L30, L90 and L180 sample after leaching at 30, 90 and 180 min. respectively. Bulk from Corsaro and Miraglia (2007).

Sample	G19 A	G19 B	STEC A	STEC B	STEC C	BEL3 A	FIA A	STEC D	STEC E	BEL3 B	BEL3 C	FIA B	Bulk glass
Grainsize (μm)	>500	<500	>500	<500	<63	<500	<500	<500	<500	<500	<500	<500	–
Treatment	UL	UL	UL	UL	UL	UL	UL	L30	L180	L30	L90	L90	–
Si	5.85	7.21	5.73	4.58	9.74	6.10	9.08	10.54	10.97	12.02	12.70	12.14	47.14
Ti	n.m.	n.m.	2.23	1.96	1.63	1.18	1.39	4.26	4.33	2.42	0.00	2.66	1.39
Al	19.73	17.50	17.35	13.33	18.20	14.68	28.18	26.03	28.80	25.09	27.20	17.05	18.79
Fe	9.47	8.03	15.80	11.65	9.39	10.50	13.60	29.05	26.82	13.36	15.13	15.55	7.35
Mg	n.m.	n.m.	4.10	4.90	2.12	3.29	3.81	n.m.	3.12	3.36	n.m.	1.87	5.70
Ca	0.72	0.55	1.68	1.65	1.79	1.08	1.51	1.78	1.94	0.72	1.25	0.98	8.49
Na	2.45	1.68	2.26	2.76	1.60	0.82	0.90	0.99	1.04	0.61	0.92	0.56	7.66
K	1.09	0.94	0.52	0.88	0.71	0.38	0.45	0.25	0.36	0.32	0.17	0.19	3.48
Cl	0.75	0.70	0.41	0.43	0.35	0.67	0.45	n.d.	0.27	0.32	0.67	0.28	n.m.
S	36.02	41.72	7.85	17.20	8.24	3.34	2.37	n.d.	4.11	3.47	3.51	1.07	n.m.

F	22.86	21.68	42.07	40.66	46.22	40.61	13.72	8.35	17.02	16.97	16.76	6.21	n.m.
N	1.06	n.d.	n.d.	n.d.	n.d.	n.d.	1.09	n.d.	1.22	1.81	n.d.	1.49	n.m.
C	n.m.	n.m.	n.m.	n.m.	n.m.	17.35	23.44	18.76	n.m.	19.53	21.69	39.93	n.m.
Sum	100	100	100	100	100	100	100	100	100	100	100	100	100

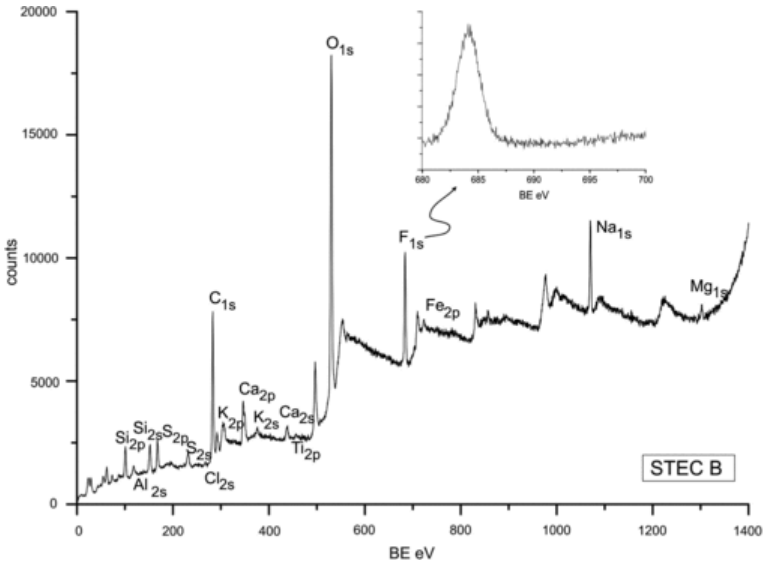

Fig. 3 XPS surface spectra of sample STEC/B. In the inset the F_{1s} peak.

All analyzed samples exhibit high S and F abundance while, among halogens, Cl values are considerably lower. Nitrogen is present on samples G19/A, FIA/A, STEC/E, BEL3/B and FIA/B while C was measured on samples BEL3/A, FIA/A, STEC/D, BEL3/B, BEL3/C and FIA/B. The abundances of volatile elements (sum of S, F, Cl, N ranging from 50.33% to 64.09%) and the elements ratios F/S (from 0.52 to 5.61) and F/Cl (from 30.30 to 131.09) are strongly variable Regarding the major elements, Si, Mg, Ca, Na and K have lower abundances than bulk glass composition (Table 3), on the contrary Fe shows higher values while Al contents are comparable.

Fluorine and sulfur contents, in particular, appear to be very high if they are compared with the abundance of alkali and alkaline earth elements at the ash surfaces. The F_{1s} and $S_{2p3/2}$ binding energies, determined in the high resolution regions, are 686.25 eV and 169.60 eV respectively and clearly indicate an ionization state -1 for the fluorine and +6 for the sulfur. Then we can suppose that these elements exist as fluorides and sulfates. Nevertheless, some HF can be physisorbed and/or complex species such as SiF_6^- can be formed on the grain surfaces.

The depletion and enrichment pattern of the surface elements have been investigated by means of the Enrichment Factor (EF):

$$\mathrm{EF} = \frac{X_s/\mathrm{Ti}_s}{X_b/\mathrm{Ti}_b}$$

In which X_s and X_b are the elements values on the surface and on the bulk glass respectively and Ti_s and Ti_b are Ti abundances in the surface and bulk glass. Ti was chosen as the normalizing element since it constitutes the least mobile element when taking into account that Al abundance, in the presence of F, may be modified by the formation of AlF_3 (White and Hochella, 1992).

The unleached samples analysed (excluding the G19B and G19A samples in which Ti was not determined) have similar EF pattern (Fig. 4a) with strong depletions of Si, Ca, Na and K, unchanged or lower Mg abundances and slight enrichments of Al and Fe. On the whole, the EF patterns are very different to the surface EF measured on the 2010 and 2011 ashes erupted by Eyjafjallajökull (Gislason et al., 2011) and Grímsvötn (Olsson et al., 2013) respectively (Fig. 4a and b).

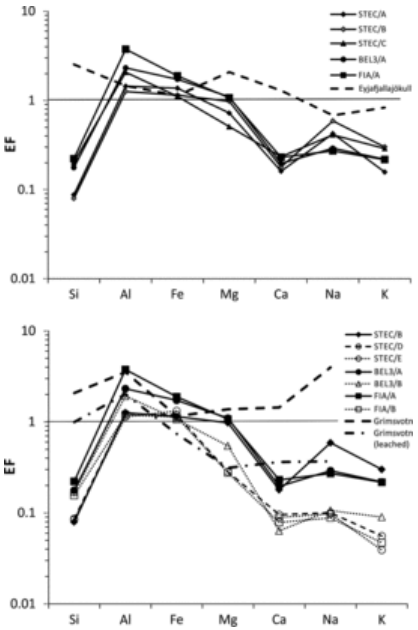

Fig. 4 Enrichment Factor (EF) spider diagrams. (A) Unleached samples. For comparison are reported the EF trend calculated for ash of 2011 Eyjafjallajökull eruption (Gislason et al., 2011). (B) Comparison between selected unleached samples (full symbols: STEC/A, BEL3/A and FIA/A) and the same samples after leaching experiments (open symbols). For the details of leaching conditions see Table 3.

In the leached samples, halogens and S abundances are considerably lower with respect to unleached samples (Table 3). Furthermore, EF (Fig. 4b) indicate that leaching produces strong depletions in the abundance of alkaline and earth alkaline elements at the surface, while Si, Al and Fe content do not change significantly. Similar behavior is reported in the XPS spectra of leached Grímsvötn ash, which demonstrate the greatest depletions in Mg, Ca and Na (Olsson et al., 2013).

3.3 TEM data

The high-resolution surface alterations of ash particles were investigated via TEM analyses. We selected glassy particles with no evidence of crystallization, with clear, homogeneous surfaces without evidence of etching or other alteration, such as that reported for hydrated volcanic glass (Kazue Tazaki et al., 1992). Droplet-shaped particles, with a diameter ranging from 100 to 200 nm (Fig. 5a), are present on the surface. The high magnification images (Fig. 5b) show that droplets are frequently polycrystalline. Furthermore, voids are sometimes observable inside the droplets (Fig. 5b) probably due to the evaporation of water in the high vacuum TEM tube or during the Ar mill thinning of the sample. Spot chemical analyses indicate that the droplets comprise NaCl (Fig. 6a), KCl, Ca and Mg sulfates, possibly in an hydrated state. The features of these particles resemble those of droplets collected on eruptive clouds (Rose et al., 1980). Patchy aggregates with sub-rounded shape (Fig. 5c) and composed principally of F, S, Ca, Mg and in minor amount Si and Al (Fig. 6b) are also present on the surface. In this case, the contact interface with the glassy particle is not sharp and is probably marked by a reaction zone. Finally, angular or sub-angular particles are settled on the surface. In most cases these particles are comprised of a single crystal (halite and sylvite in Fig. 5c and d) or by aggregates of these phases (Fig. 5f).

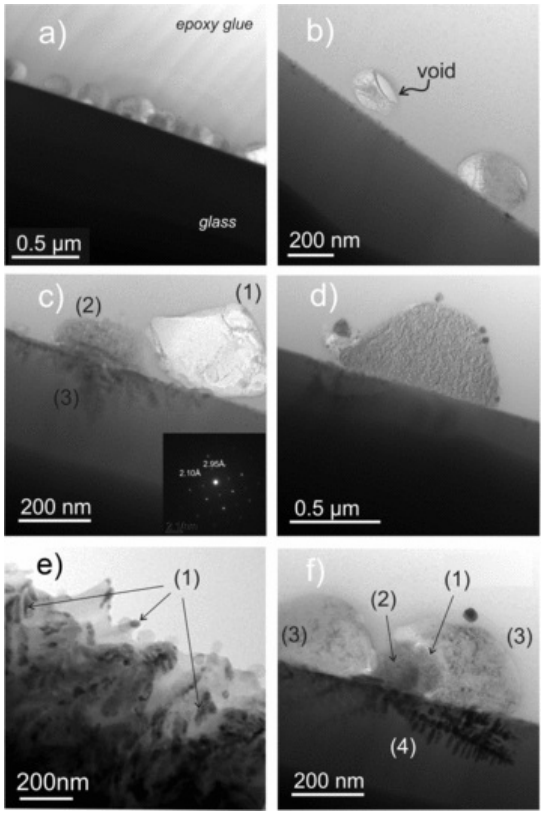

Fig. 5 TEM photographs; (a) particle surface (dark grey) covered by numerous NaCl droplets; (b) high magnification image of droplets with polycrystalline structure, inside the smaller droplet is observable a void with concave shape; (c) sub-angular NaCl settled on the surface (1) and patchy aggregates with sub-rounded shape formed by sulphate (hydrated?) and fluorides (2). In the insert it is shown the diffraction pattern of magnesioferrite visible as dendrites under the surface (3); (d) KCl euhedral crystal on the surface; (e) magnesioferrite and native iron (1) dendrites; (f) Ca, Fe, Mg fluoride (1) rounded by Ca, Mg sulphate (hydrated?) (2) and NaCl (3). The magnesioferrite dendrites (4) are bigger than in (c).

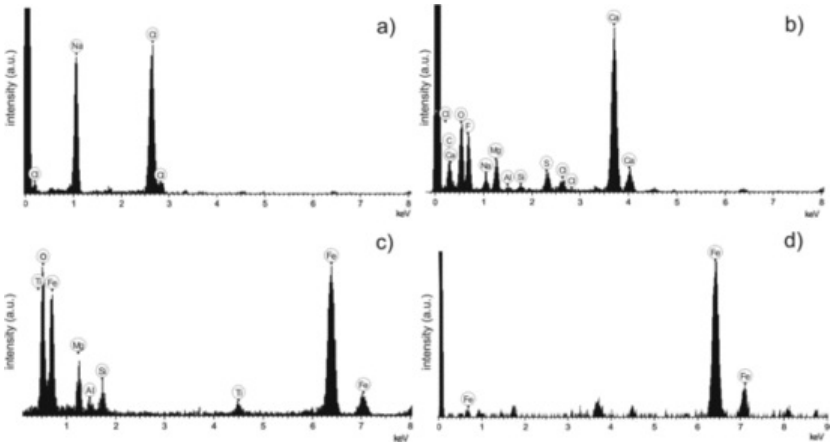

Fig. 6 TEM-EDS spot analysis of: (a) NaCl droplet; (b) patchy rounded aggregate; (c) magnesioferrite dendrites; (d) native iron bearing region of dendrite.

TEM images also frequently highlight dendritic nanometric (~10 nm) magnesioferrite (insert in Fig. 5c and f; Fig. 6c) crystals growing beneath the surface of glassy particles. Sometimes, in coincidence with F–S bearing patchy aggregates or epitaxies, larger magnesioferrite crystals (on average ~200 nm) are observed. This behavior suggests an enhanced (epitaxial) accelerated crystal growth at the interface between glassy particles and the overlying crystals as observed also in obsidian, during early devetrification processes (Gimeno, ~~2004~~2003).

Notably, small areas containing large magnesioferrite dendrites of metallic iron are observed, evidenced by spot chemical analyses in which only the Fe peaks are observable (Figs. 5e and 6d). The presence of magnesioferrite and metallic iron on the glassy particles offers a possible explanation for the lack of an Fe-depleted ash surface, previously characterized as common to XPS-analysed ash surface (Delmelle et al., 2007; Ayris and Delmelle, 2012b).

The variation of glassy composition close to the surface is described by four EDXS elements profiles performed with TEM on glassy particles from different samples. This technique is complementary to the XPS analysis, providing the chemical composition at greater depth from the surface than that probed by XPS, although it does not permit the investigation of the chemical variation within the 1 to 5 nm thick layer probed by XPS, as EDXS has a 10 nm spatial resolution. The results, shown in Fig. 7, indicate that: (i) Si and, in smaller amount, Al abundances gradually decrease from ~100 nm to the surface; (ii) Fe, Mg and Ca contents increase from ~150 nm toward the surface; (iii) F shows high variability and becomes more abundant from ~50 nm toward the surface; (iv) Ti and S abundances do not change in the profile.

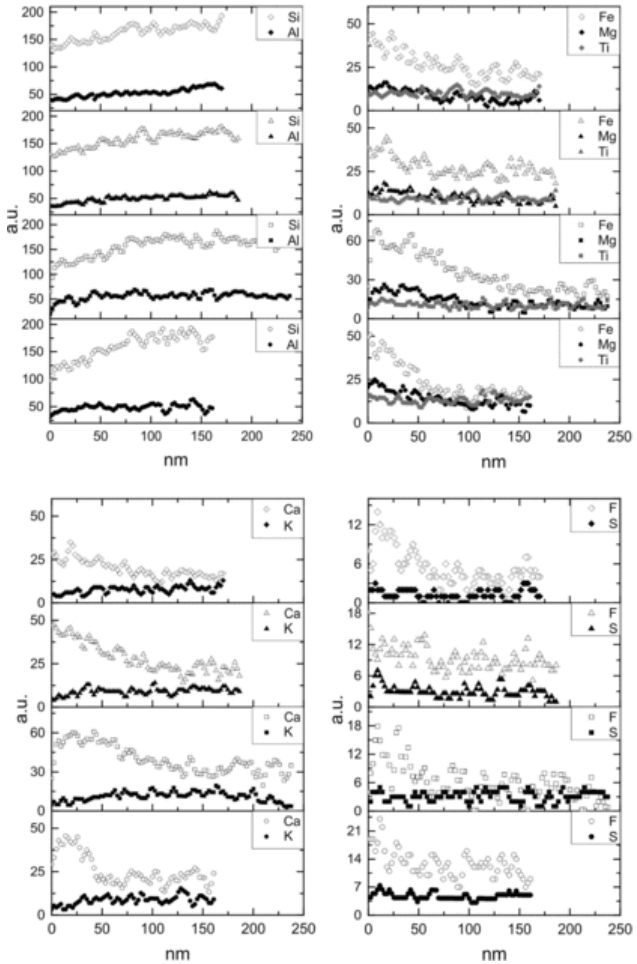

Fig. 7 TEM compositional profiles of different elements depending on the distance from the surface (=0 nm) of the ash particle.

Indications of reactive contact between F and S compounds and the glassy surface are highlighted in chemical profiles of Fig. 8. Starting from the inner region of the ash fragment, it is possible to distinguish: (1) fresh volcanic glass; (2) a zone with high

Fe and low F with magnesioferrite dendrites; (3) a region close to the surface (indicated as 0 nm) with high Fe and F and decreasing Si and Al; (4) the interface between the glass and an overlying patchy aggregate with lower Fe, Si and Al, high F and increasing Ca; (5) the intermediate region of the patchy aggregate with a strong increase of Ca, F and S and low Si, Al and Fe abundances; (6) small (10 nm) droplet marked by high Ca content and S/F ratio; (7) a more external region of the particle with different composition due to high S and Ca; (8) small droplet with high Ca and lower S and F.

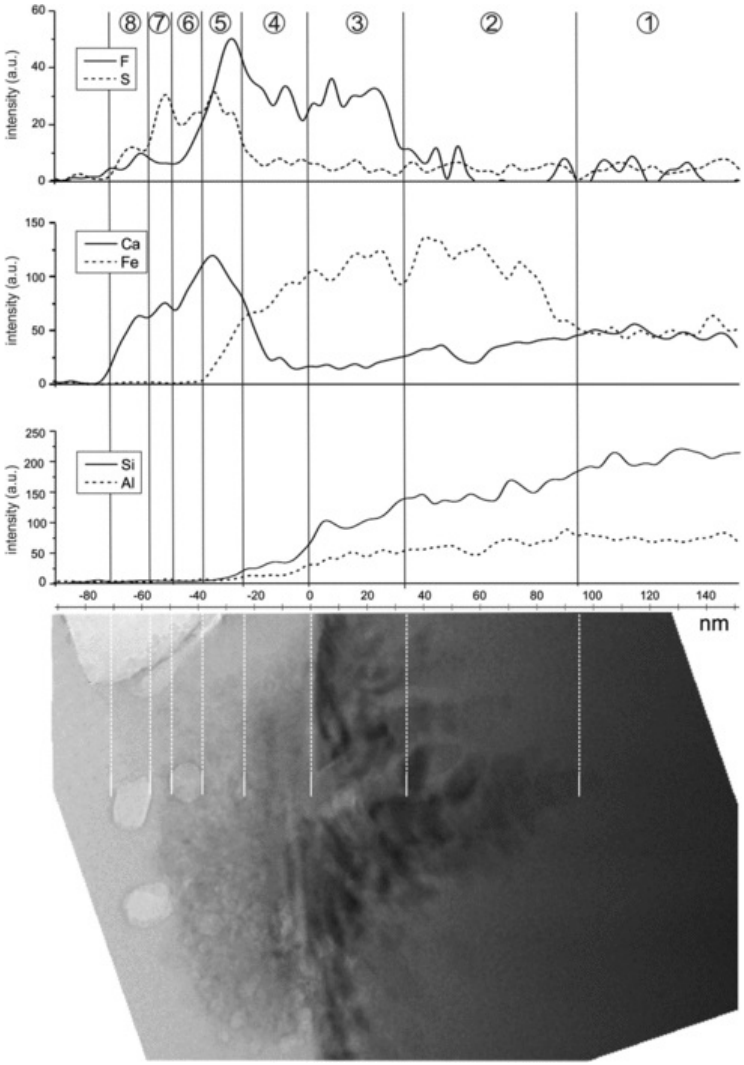

Fig. 8 TEM compositional profile crossing ash particle external rim with magnesioferrite dendrites, an overlying patchy aggregates and droplet particle. The surface of the ash particle is aligned by 0 nm in the distance scale.

4 Discussion

The results obtained with different analytical methods highlight a number of different processes that together, concur to modify the glassy particle surfaces. Óskarsson (1980) proposed a plume model in which the interaction between the ash particles and the aerosol occurs in zones characterized by different physical – chemical conditions. However, we argue here that the modification of the surfaces of tephra may begin before the eruption, since most of the surface of ash shards correspond to the original contact area between gas bubbles and melt during magma ascent in the conduit. The different phases of the complex ashes modifications described in the following sections are schematically illustrated in Fig. 9.

4.1 Pre-eruptive processes

EDXS profiles evidenced the peculiar distribution of volatile elements at the ash surface. Above the glassy surface of the particles, Cl, S and F are detected in discrete domains, generally in the form of chlorides, sulphates and fluorides (Figs. 5 and 8). Relatively high abundances of all these elements are also revealed by XPS analyses performed from the surface to the inner part of the particles. Below the particle surface, the concentration of volatile elements follows a different distribution. Chlorine and S concentrations rapidly decrease with increasing depth within the sample (Fig. 8). Fluorine, on the contrary, is present on the glassy surface but shows a gradual decrease (Figs. 7 and 8) over a depth of about ~50 nm into the particle interior. This trend resembles a diffusion process, but rather than an exsolution pattern, which implies that volatiles decrease from the inside to the surface, this instead suggests the migration of this element from the particle exterior to the interior.

As diffusion is enhanced at high temperature (Baker et al., 2005), this strongly suggests that the inward diffusion of F principally occurs before the eruption, as after fragmentation and during subaerial emission, tephra experience near magmatic temperatures only for a very short period.

Elemental profiles, as that observed for F in the external layer of ash particles (Fig. 8), are reported in literature for H_2O dissolved in tephra and have been interpreted as typical of resorption process (Watkins et al., 2012). Furthermore, Carey et al. (2013) supports the hypothesis of resorption of volatiles by melts on the basis of indirect evidence provided by bubble resorption in basaltic clasts. In both cases, the resorption process is considered by the authors to be driven by an increase of pressure, but more recently (McIntosh et al., 2014) proposed that a magma temperature decrease could yield the same compositional profile shape, due to the inverse relationship between temperature and volatile solubility in the melt.

The widespread knowledge of volatile behavior at Mt. Etna constitutes a good basis for the comprehension of pre-eruptive magma-gas interactions. Melt inclusion analysis constrained the pressure at which volatiles separate from the melt during recent Mt. Etna eruption (Spilliaert et al., 2006), evidencing that F exsolution begins at ⩽10 MPa (~0.4 km below the summit vents; Fig. 9A) while Cl exsolves at ⩽100 MPa (~4.1 km) and sulfur at ⩽140 MPa (~5.30 km). The shallow exsolution of F is consistent with the smaller ionic radius of this element with respect to Cl that determines major affinity of F in the silicate melts.

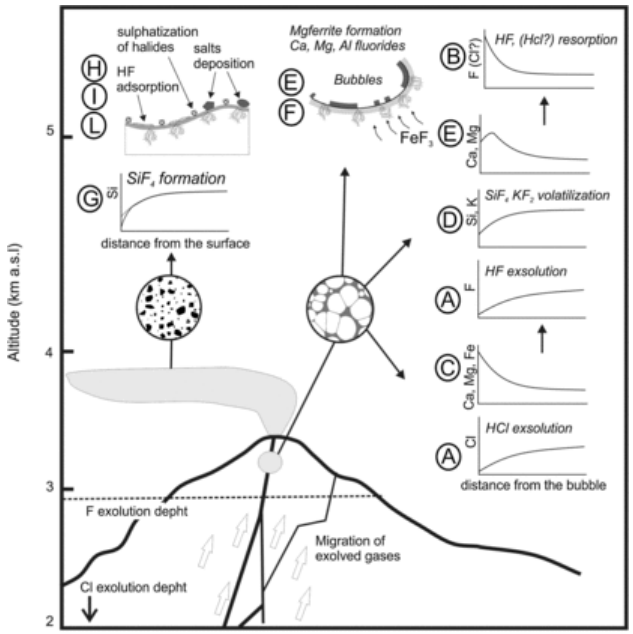

Fig. 9 Cartoon showing the interaction processes occurring between melt/ash and volatile phases in Mt. Etna volcanic system. Details are reported in the text.

Therefore, the gas/melt pressure and temperature variations may change partition coefficients permitting the resorption of halogens (principally of F and subordinately of Cl) in the melt (Fig. 9B).

We envisage that a combination of pressure increase, temperature decrease and volatile composition may have determined the observed element distribution in Etna volcanic glasses. Melnik et al. (2005) have shown that overpressure may build-up along the volcanic conduits as a consequence of an increase in the bubble viscous resistance thus driving volatile resorption during the magma ascent. In addition, concomitant temperature decrease can contribute to increasing volatile solubility in the melt (McIntosh, 2013). Finally, since halogens partitioning between fluid and melt is highly dependent by the composition of the fluid phase, as highlighted by Alletti et al. (2006), it cannot be excluded that resorption in the melt may then be influenced by migration of,

CO_2, SO_2 and, in particular, H_2O from depth. It is worth noting that Ferlito et al. (2014) considered the H_2O flux through the plumbing system and its absorption by water-undersaturated magma as the main mechanism feeding the persistent gas plume of Mt. Etna summit craters.

In this context, the F features in the Mt. Etna glasses registered by TEM profiles are interpretable through a first F exsolution (>0.4 km below the summit vents) followed by F re-sorption in the upper part of the conduit.

The behavior of halogens during the magma ascent may be responsible for the outward migration of Ca, Mg and Fe observed in the TEM profiles (Figs. 7 and 8) with a mechanism similar to that proposed by Ferlito and Lanzafame (2010). Chlorine ions dissolved in the melt are able to form metal complexes (Africano and Bernard, 2000). As pressure decreases Cl^- complexes migrate toward the bubble wall and upon halogen exsolution as HCl the metals remain within the melt. This can account for the observed metal enrichment in the melt layer close to bubble wall surfaces (Fig. 9C). In the case of K, the strong affinity of this element with halogens results in the volatilization of KF and KCl (Fig. 9D) thus explaining the outward K decrease observed in the TEM profiles (Figs. 7 and 8). This hypothesis would be consistent with the presence of potassium in the solid aerosol sampled during Mt. Etna 1983 eruption and originated by condensation (Quisefit et al., 1988).

The presence of SiF_4 in Mt. Etna volcanic gases has been reported in literature (Francis et al., 1996) suggesting that the volatilization of this compound is responsible for the outward decrease in Si abundance observed in the TEM profiles (Fig. 9D). Rosenberg (1973) considers the SiF_4 formation as a low temperature process and White and Hochella (1992), on the basis of thermodynamic considerations, demonstrated that Si volatilization by means of SiF_4 formation is relevant at $T < 375$ °C for the reaction:

$$SiO_2 + 4HF \rightarrow SiF_4 + 2H_2O \quad (1)$$

Similar reactions may produce minor amount of less volatile SiF_6.

However, the same authors suggested that SiF_4 can be produced at higher temperature (>550 °C) through more complex reaction in which other elements, in addition to Si, are involved are involved:

$$Al_2SiO_5 + 10HF \rightarrow 2AlF_3 + SiF_4 + 5H_2O \quad (2)$$

$$CaSiO_3 + 6HF \rightarrow CaF_2 + SiF_4 + 3H_2O \quad (3)$$

$$Mg_2SiO_4 + 8HF \rightarrow 2MgF_2 + SiF_4 + 4H_2O \quad (4)$$

In all of these reactions SiF_4 is volatile under low pressure and temperature conditions (sublimation temperature of SiF_4 is –86 °C at 1 bar pressure) while AlF_3, CaF_2 and MgF_2 (sublimation temperatures are respectively 1225, 2300 and 2200 °C at 1 bar pressure) remain as solid phases (Fig. 9E) as those observable in the region (4) of the Fig. 8 TEM image and profile. This process may be enhanced by Na^+, Mg^{2+} and Ca^{2+} diffusion from particle interiors to their surfaces (Ayris et al., 2013, 2014).

A similar reaction can describe the formation of SiF_4 at high temperature and in presence of Fe:

$$Fe_2SiO_4 + 10HF + 1/2O_2 \rightarrow FeF_3 + 4SiF_4 + 5H_2O \quad (5)$$

However, this reaction should cause depletion of Si and Fe because SiF_4 and FeF_3 are volatile at high temperature.

In this scenario, the manifold magma-halogens interaction occurring during magma ascent within the conduit, may cause the formation of the magnesioferrite dendrites observed close to the surface of the glassy particles. These spinels are unlikely crystallised from the Etna magma, as magmatic oxide phases are typically Ti-magnetite (Corsaro and Pompilio, 2004). Magnesioferrite probably formed, instead, via the reaction between volcanic rocks and hot gases (Bowles et al., 2011) as suggested by its presence within fumarolic deposits of Vesuvio and Etna (Cipriotti et al., 2009). Draper (1935) synthesized magnesioferrite by HCl gas reaction with FeO and MgO at near magmatic temperature (800–950 °C), initially producing gaseous $FeCl_2$ that subsequently reacted with MgO to yield $MgFe_2O_4$ and Cl_2. In our case, the magnesioferrite could be formed via a similar reaction pathway that started with the volatilization of FeF_3 (Eq. (5)) (Fig. 9F). Alternatively, magnesioferrite formation may be caused by oxidation of Fe^{2+} to Fe^{3+} (Ayris and Delmelle, 2012b) occurring during in plume transport of ash particles. This process prompts some structural modification of the glass network in which the tetrahedral coordination of Fe^{3+} is enabled by the compensation of the negative charge by alkali cations. However, if alkaline cations are not available, oxidation can cause the formation of discrete Fe^{3+} bearing phases, such as spinels (Cook et al., 1990; Cooper et al., 1996). The presence, never reported in literature, of nanometric metallic iron in large magnesioferrite dendrites would be indicative of the local achievement of very low oxygen fugacity conditions. A straightforward origin for the metallic Fe detected in our samples is, at the moment, not yet well defined although the presence of Fe^0 in magmas has been described elsewhere. While metallic Fe is rather unusual for terrestrial rocks, disseminated globules of Fe^0 with a drop-like shape, have been in fact be described in volcanic rocks in the past years (Melson and Switzer, 1966). They are generally ascribed to the magma interaction, and consequent assimilation, with coal-bearing sedimentary rocks (Klöck et al., 1986; Kamenetsky et al., 2013). Actually, the presence of Fe^0 in close association to magnesioferrite crystals, rather than as randomly distributed (micro)droplets, contrasts with this hypothesis. Recently, high levels of Fe^{+3} are observed in silicate perovskite in chemical equilibrium with metallic iron (Frost et al., 2004). These authors suggest that that silicate perovskite appropriates oxygen either by the reduction of volatile species or by the disproportionation of Fe^{+2} to Fe^{+3} and metallic Fe. Although speculatively, this latter process could be invoked for the Fe^0 domains found in close spatial association with magnesioferrite in our samples.

4.2 Processes in the plume

According to most literature, we propose that the interaction among ash particles and gases continue in the plume where different conditions exist, depending on the distance from the eruptive vent (Óskarsson, 1980). Delmelle et al. (2007) stated that these chemical depletion and enrichment processes are caused by acid dissolution. In particular, the presence in the plume of F (Fig. 9G), in both the gas and liquid phases suggest the production, according the reaction (1), of volatile SiF_4. However, this process

require that the ash particles stay on at high temperature region of the plume for a time sufficient to allow the surface alteration. The timescale of gas/ash interaction at 200 °C, considered congruent with the SiF_4 volatilization (Rosenberg, 1973; White and Hochella, 1992), was calculated using magma discharge rates of 10^5 kg/s suggested by Bonaccorso et al. (2014) for the November 2013 Mt. Etna activity. The plume cooling rate calculated by Ayris et al. (2014) for explosive eruptions with similar magma discharge rates (10^6 kg/s) suggests the persistence of the ashes at 200 °C for <10 s. This short time lapse allows us to invoke the occurrence of in-plume processes only for minor Si depletion interesting the few nanometric thick external layer, and indirectly to confirm that actually the chemistry of ash particles was modified mainly during pre-eruptive stages. However, some of the ash surface features show that further reactions occur in the plume. In particular, the very high F and S abundances on the surface, uncoupled with Ca, Mg, Na and K highlighted by XPS analysis, suggest the presence on the surface of physisorbed HF (Fig. 9H). This hypothesis is supported by the considerable decrease of pH in the first seconds of the leaching experiments (see X-ray photoelectron spectroscopy in "Materials and methods" paragraph). Moreover, halide salts may continuously react with SO_2 and H_2O and may form sulphates according to the reactions 2XF (solid) + H_2SO_4 (liquid) ↔ X_2SO_4 (solid) + 2HF (gas) and 2XCl (solid) + H_2SO_4 (liquid) ↔ X_2SO_4 (solid) + 2HCl (gas) proposed by Toutain et al. (1995) for the sulphatization of chlorides (Fig. 9I).

The picture is complicated by the adhesion of salts (NaCl, KCl, Ca and Mg sulphates) on ash surfaces, droplets and crystals that, according with Óskarsson (1980) are formed directly by condensation of gases in the plume without evidences of chemical exchanges with the glass (Fig. 9L).

Finally, the presence on the surface of soluble salts, physisorbed HF and the hydrolysis of the complex species such as SiF_6^- yielding silica and hydrofluoric acid may explain the solubilization of F, S and alkaline and earth alkaline elements registered by XPS after the leaching experiments.

It is noteworthy that the picture we have drawn is based on the observations carried out on ashes emitted during recent lava fountains at Etna, but substantial differences of the superficial composition may be produced by various eruptive styles. For example, our data show meaningful differences when compared with samples collected by Delmelle et al. (2007) during the long-lasting ash emission associated with the Etna 2001 flank eruption. In particular, the composition of Delmelle's samples analyzed with XPS, might be different from ours because the ash was erupted on 2–3 August 2001 (see Table 1 in Delmelle et al., 2007). In that period the activity shifted from magmatic to phreatomagmatic (Behncke and Neri, 2003) and produced the continuous emission of lithic ash (Corsaro et al., 2007) poorer in volatile components (S, F, Cl) thus a definitely different ash with respect that one considered in our study. Also the comparison between the compositions of ash erupted by Etna and other volcanoes, such as Eyjafjallajökull (Gislason et al., 2011) in 2010 and Grímsvötn (Olsson et al., 2013) in 2011, evidences different EF of major elements thus hindering any obvious parallelism between these ashes due to their deeply different nature.

These observations bring the attention to some aspects that may deserve some attention in the next, i.e., the role played by the different type of volcanic activity and original gas composition in controlling gas-ash interactions and in modifying composition of ash particle.

5 Conclusion

The outcomes of the present paper provide insights into the complex processes which modify the surface of Mt. Etna ash emitted during the 2013 paroxysmal activity at the New South East Crater. The chemical and mineralogical composition of ash particles have been investigated at a nanometric scale via TEM and XPS observations. The intricate effects of interaction between volatile elements and the ash surface allow to us to propose multistage process operating under variable P and T conditions. The compositional modification begins in the shallow plumbing system (T~1100 °C, P < 100 MPa) due to the exsolution and resorption of F^- occurring at the bubble-melt interface, which represents a proto-surface of the future ash particle. During this stage, halogens form compounds with Si, K Fe, Ca and Mg of the melt and, in function of their volatility, cause Si and K depletion and Fe, Ca and Mg enrichment in the layer close to the bubble. Iron is fixed as magnesioferrite and metallic iron crystallizing as nanometric dendrites under the surface.

In the plume, the particle surface is further modified principally by physisorbed HF, by continuous partial transformation of sulphates and halides and by the dissolution of soluble phases in response to the changes of chemical and physical conditions.

Although the reactions occurring between gases/aerosols and basaltic volcanic ash particles remains poorly understood, our study, concerning the surface physic-chemical properties of ash, improves current understanding of the key processes at work in eruptive and pre-eruptive environments.

We highlighted the important role of gas/aerosol–ash interaction in modifying the surface of ash particles. The chemical and mineralogical surface features we identify may play a key role in the determination of ash behavior in the receiving environments, and may influence the alteration of volcanic glasses in subaerial and subaqueous conditions (Parruzot et al., 2015). Moreover, the understanding of surface processes provides an indispensable basic knowledge to improve the assessment of potential threats for human/animal health and agricultural activities. With this respect, the recent study by Horwell et al. (2007) has assessed the high activity of Mt. Etna ash with respect to the hydroxyl radical generation. This activity was particularly linked to the presence of Fe(II) and Fe(III) in the ashes. Here, the Fe speciation between glass, magnesioferrite and Fe, and the occurrence of nanostructure of Fe-bearing phases surely yield this picture more complex. Further studies are in progress to exactly define the Fe speciation, in order to contribute to ascertain the role of the different Fe species with respect to the health effects.

Acknowledgment

We thank Paul Ayris and two anonymous reviewers whose comments permitted us to improve this paper. We would like to thank Dr. D. Lo Castro who performed the grain size analysis with CAMSIZER® at INGV Catania laboratories.

This study was funded by MIUR (Italy) PRIN 2010/2011 project prot. 2010MKHT9B.

References

Africano F. and Bernard A., Acid alteration in the fumarolic environment of Usu volcano, Hokkaido, Japan, *J. Volcanol. Geoth. Res.* **97**, 2000, 475–495.

Alletti M., Aiuppa A., Baker D.R. and Freda C., Fluid/melt partitioning coefficients of chlorine in basaltic melt, *Geophys. Res. Abstr.* **8**, 2006, 08823.

Andronico D. and Corsaro R.A., Lava fountains during the episodic eruption of South-East Crater (Mt. Etna), 2000: insights into magma-gas dynamics within the shallow volcano plumbing system, *Bull. Volcanol.* **73**, 2011, 1165–1178.

Andronico D., Scollo S., Lo Castro M.D., Cristaldi A., Lodato L. and Taddeucci J., Eruption dynamics and tephra dispersal from the 24 November 2006 paroxysm at South-East Crater, Mt Etna, Italy, *J. Volcanol. Geoth. Res.* **274**, 2014, 78–91.

Ayris P.M. and Delmelle P., The immediate environmental effects of tephra emission, *Bull. Volcanol.* **74**, 2012a, 1905–1936.

Ayris P.M. and Delmelle P., Volcanic and atmospheric controls on ash iron solubility: a review, *Phys. Chem. Earth Part A.* **45–46**, 2012b, 103–112.

Ayris P.M., Lee A.F., Wilson K., Kueppers U., Dingwell D.B. and Delmelle P., SO_2 sequestration in large volcanic eruptions: high-temperature scavenging by tephra, *Geochim. Cosmochim. Acta* **110**, 2013, 58–69.

Ayris P.M., Delmelle P., Cimarelli C., Maters E.C., Suzuki Y.J. and Dingwell D.B., HCl uptake by volcanic ash in the high temperature eruption plume: mechanistic insights, *Geochim. Cosmochim. Acta* 2014.

Baker D.R., Freda C., Brooker R.A. and Scarlato P., Volatile diffusion in silicate melts and its effects on melt inclusions, *Ann. Geophys.* **48**, 2005, 699–717.

Barone G., Ciliberto E., Costagliola P. and Mazzoleni P., X-ray photoelectron spectroscopy of Mt. Etna volcanic ashes, *Surf. Interface Anal.* **46**, 2014, 847–850.

Behncke B., Branca S., Corsaro R.A., De Beni E., Miraglia L. and Proietti C., The 2011–2012 summit activity of Mount Etna: birth, growth and products of the new SE crater, *J. Volcanol. Geoth. Res.* **270**, 2014, 10–21.

Biass S., Scaini C., Bonadonna C., Folch A., Smith K. and Höskuldsson A., A multi-scale risk assessment for tephra fallout and airborne concentration from multiple Icelandic volcanoes – Part 1: Hazard assessment, *Nat. Hazards Earth Syst. Sci.* **14**, 2014, 2265–2287.

Bonaccorso A., Calvari S., Linde A. and Sacks S., Eruptive processes leading to the most explosive lava fountain at Etna volcano: the 23 November 2013 episode, *Geophys. Res. Lett.* **41**, 2014.

Bowles J.F.W., Vaughan D.J., Howie R.A. and Zussman J., *Rock-Forming Minerals Vol. 5A Non-Silicates: Oxides, Hydroxides and Sulphides* 2011, Geological Society of London; UK.

Briggs D. and Beamson G., Primary and secondary oxygen-induced C1s binding energy shifts in x-ray photoelectron spectroscopy of polymers, *Anal. Chem.* **64**, 1992, 1729–1736.

Carey R.J., Manga M., Degruyter W., Gonnermann H., Swanson D., Houghton B., Orr T. and Patrick M., Convection in a volcanic conduit recorded by bubbles, *Geology* **41**, 2013, 395–398.

Cipriotti, M. E., Fascio, L., Pasero, M. (2009). Italian type minerals. Edizioni Plus, Pisa.

Cook G.B., Cooper R.F. and Wu T., Chemical diffusion and crystalline nucleation during oxidation of ferrous iron-bearing magnesium aluminosilicate glass, *J. Non-Cryst. Solids* **120**, 1990, 207–222.

Cooper R.F., Fanselow J.B. and Poker D.B., The mechanism of oxidation of a basaltic glass: chemical diffusion of network modifying cations, *Geochim. Cosmochim. Acta* **60**, 1996, 3253–3265.

Corsaro R.A. and Miraglia L., Dynamics of 2004–2005 Mt. Etna effusive eruption as inferred from petrologic monitoring, *Geophys. Res. Lett.* **32**, 2007.

Corsaro R.A. and Miraglia L., The transition from summit to flank activity at Mt. Etna, Sicily (Italy): inferences from the petrology of products erupted in 2007–2009, *J. Volcanol. Geoth. Res.* **275**, 2014, 51–60.

Corsaro R.A. and Pompilio M., Magma dynamics in the shallow plumbing system of Mt. Etna as recorded by compositional variations in volcanics of recent summit activity (1995–1999), *J. Volcanol. Geoth. Res.* **137**, 2004, 55–71.

Delmelle P., Lambert M., Dufrêne Y., Gerin P. and Óskarsson N., Gas/aerosol–ash interaction in volcanic plumes: new insights from surface analyses of fine ash particles, *Earth Planet. Sci.* **259**, 2007, 159–160.

Draper R.B., The synthesis of magnesioferrite and observations on “mineralization”, *Am. J. Sci.* **30**, 1935, 106–115.

Fairley N., XPS lineshapes and curve fitting, In: Briggs D. and Grant J.T., (Eds.), *Surface Analysis by Auger and X-ray Photoelectron Spectroscopy,* 2003, IM Publications; Chichester, UK, 398.

Fano F., Cernigliaro A., Scondotto S., Perucci C.A. and Forastiere F., The fear of volcano: short-term health effects after Mount Etna's eruption in 2002, *Eur. Respir. J.* **36**, 2010, 1216–1218.

Ferlito C. and Lanzafame G., The role of supercritical fluids in the potassium enrichment of magmas at Mount Etna volcano (Italy), *Lithos* **119**, 2010, 642–650.

Ferlito C., Coltorti M., Lanzafame G. and Giacomoni P.P., The volatile flushing triggers eruptions at open conduit volcanoes: evidence from Mount Etna volcano (Italy), *Lithos* **184–187**, 2014, 447–455.

Francis P., Chaffin C., Maciejewski A. and Oppenheimer C., Remote determination of SiF4 in volcanic plumes: a new tool for volcano monitoring, *Geophys. Res. Lett.* **23**, 1996, 249–252.

Frost D.J., Liebske C., Langenhorst F., McCammon C.A., Trønnes R.G. and Rubie D.C., Experimental evidence for the existence of iron-rich metal in the Earth's lower mantle, *Nature* **428**, 2004, 409–412.

Gimeno D., Devitrification of natural rhyolitic obsidian glasses: petrographic and microstructural study (SEM+EDS) of recent (Lipari island) and ancient (Sarrabus, SE Sardinia) samples, Journal of Non-Crystalline Solids **323**, 2003, 84-90.Gislason S.R., Hassenkam T., Nedel S., Bovet N., Eiriksdottir E.S., Alfredsson H.A., Hem C.P., Balogh Z.I., Dideriksen K., Oskarsson N., Sigfusson B., Larsen G. and Stipp S.L.S., Characterization of Eyjafjallajökull volcanic ash particles and a protocol for rapid risk assessment, *PNAS* **108**, 2011, 7307–7312.

Gualtieri A.F., Accuracy of XRPD QPA using the combined Rietveld-RIR method, *J. Appl. Cryst.* **33**, 2000, 267–278.

Horwell C.J., Fenoglio I. and Fubini B., Iron-induced hydroxyl radical generation from basaltic volcanic ash, *Earth Planet. Sci. Lett.* **261**, 2007, 662–669.

Kamenetsky V.S., Charlier B., Zhitova L., Sharygin V., Davidson P. and Feig S., Magma chamber-scale liquid immiscibility in the Siberian Traps represented by melt pools in native iron, *Geology* **41**, 2013, 1091–1094.

Kazue Tazaki K., Tiba T., Aratani M. and Miyachi M., Structural water in volcanic glass, *Clays Clay Miner.* **40**, 1992, 122–127.

Klöck W., Palme H. and Tobschall H.J., Trace elements in natural metallic iron from Disko Island, Greenland, *Contrib. Miner. Petrol.* **93**, 1986, 273–282.

Larson, A. C., Von Dreele, R. B. (2000). General structure analysis system (GSAS). In *Laboratory* (ed. L. A. N.).

Le Maitre R.W., Igneous Rocks: A Classification and Glossary of Terms: Recommendations of International Union of Geological Sciences Subcommission on the Systematics of Igneous Rocks, 2002, Cambridge University Press.

Lo Castro, M. D., Andronico, D. (2008). Operazioni di base per la misura della distribuzione granulometrica di particelle vulcaniche tramite il Camsizer, Rapporti tecnici. INGV, Catania.

Mather T.A., Pyle D.M. and Oppenheimer C., Tropospheric volcanic aerosol, In: Robock A. and Oppenheimer C., (Eds.), *Volcanism and the Earth's Atmosphere,* 2003, American Geophysical Union; Washington, DC, 189–212.

McIntosh, I. M. (2013). Bubble growth and resorption in magma: insights from dissolved water distributions in volcanic glass. Durham University, Available at Durham E-Theses Online: <http://etheses.dur.ac.uk/8505/>.

McIntosh I.M., Llewellin E.W., Humphreys M.C.S., Nichols A.R.L., Burgisser A., Schipper C.S. and Larsen J.F., Distribution of dissolved water in magmatic glass records growth and resorption of bubbles, *Earth Planet. Sci. Lett.* **401**, 2014, 1–11.

Melnik O., Barmin A.A. and Sparks R.S.J., Dynamics of magma flow inside volcanic conduits with bubble overpressure buildup and gas loss through permeable magma, *J. Volcanol. Geoth. Res.* **143**, 2005, 53–68.

Melson W.G. and Switzer G., Plagioclase-spinel-graphite xenoliths in metallic iron-bearing basalts, Disko island, Greenland, *Am. Mineral.* **51**, 1966, 664–676.

Olsson J., Stipp S.L.S., Dalby K.N. and Gislason S.R., Rapid release of metal salts and nutrients from the 2011 Grimsvotn, Iceland volcanic ash, *Geochim. Cosmochim. Acta* **123**, 2013, 134–149.

Óskarsson N., The interaction between volcanic gases and tephra: fluorine adhering to tephra of the 1970 Hekla eruption, *J. Volcanol. Geotherm. Res.* **8**, 1980, 251–266.

Parruzot B., Jollivet P., Rébiscoul D. and Gin S., Long-term alteration of basaltic glass: mechanisms and rates, *Geochim. Cosmochim. Acta* **154**, 2015, 28–48.

Quisefit J.P., Bergametti G., Tedesco D., Pinart J. and Colin J.L., Origin of particulate potassium in the Mt. Etna emission before and during the 1983 eruption, *J. Volcanol. Geotherm. Res* **35**, 1988, 111–119.

Rose W.I., Scavenging of volcanic aerosol by ash: atmospheric and volcanologic implications, *Geology* **5**, 1977, 621–624.

Rose W.I. and Durant A.J., Fine ash content of explosive eruptions, *J. Volcanol. Geoth. Res.* **186**, 2009, 32–39.

Rose W.I.J., Chuan J.R., Cadle R.D. and Woods D.C., Small particles in volcanic eruption clouds, *Am. J. Sci.* **280**, 1980, 671–696.

Rosenberg P.E., HF/SiF_4 ratios in volcanic and magmatic gases, *Geochim. Cosmochim. Acta* **37**, 1973, 109–112.

Ruggieri F., Saavedra J., Fernandez-Turiel J.L., Gimeno D. and Garcia-Valles M., Environmental geochemistry of ancient volcanic ashes, *J. Hazard. Mater.* **183**, 2010, 353–365.

Spilliaert N., Métrich N. and Allard P., S-Cl–F degassing pattern of water-rich alkali basalt: modelling and relationship with eruption styles on Mount Etna volcano, *Earth Planet. Sci. Lett.* **248**, 2006, 772–786.

Stewart C., Horwell C., Plumlee G., Cronin S., Delmelle P., Baxter P., Calkins J., Damby D., Morman S. and Oppenheimer C., Protocol for analysis of volcanic ash samples for assessment of hazards from leachable elements, *Int. Volcanic Health Hazards Network Publ.* 2013, 1–22.

Toby B.H., EXPGUI, a graphical user interface for GSAS, *J. Appl. Cryst.* **34**, 2001, 210–213.

Toby B.H., R factors in Rietveld analysis: how good is good enough?, *Powder Diffr.* **21**, 2006, 67–70.

Toutain J.P., Quisefit J.P., Briole P., Aloupogiannis P., Blanc P. and Robaye G., Mineralogy and chemistry of solid aerosols emitted from Mount Etna, *Geochem. J.* **29**, 1995, 163–173.

Watkins J.M., Manga M. and De Paolo D.J., Bubble geobarometry: a record of pressure changes, degassing, and regassing at Mono Craters, California, *Geology* **40**, 2012, 699–702.

White A.F. and Hochella M.F., Surface chemistry associated with the cooling and suaerial weathering of recent lava flows, *Geochim. Cosmochim. Acta* **56**, 1992, 3711–3721.

Witham C.S., Oppenheimer C. and Horwell C.J., Volcanic ash-leachates: a review and recommendations for sampling methods, *J. Volcanol. Geoth. Res.* **141**, 2005, 299–326.

Queries and Answers

Query: Your article is registered as a regular item and is being processed for inclusion in a regular issue of the journal. If this is NOT correct and your article belongs to a Special Issue/Collection please contact a.mutale1@elsevier.com immediately prior to returning your corrections.
Answer: Yes, the article is a regular item

Query: Please confirm that given name(s) and surname(s) have been identified correctly.
Answer: They are correct (with the exception of R.A. Corsaro)

Query: References “Gimeno (2004)” is cited in the text but not provided in the reference list. Please provide it in the reference list or delete these citations from the text.
Answer: We added the reference in the list

Query: One or more sponsor names may have been edited to a standard format that enables better searching and identification of your article. Please check and correct if necessary.
Answer: It is right

Query: The country names of the Grant Sponsors are provided below. Please check and correct if necessary. ‘MIUR’ - ‘Italy’.
Answer: It is right